miRNA Regulation of the Hyperproliferative Phenotype of Vascular Smooth Muscle Cells in Diabetes

Daniele Torella,[1] Claudio Iaconetti,[1] Roberta Tarallo,[2] Fabiola Marino,[1] Giorgio Giurato,[2,3] Claudia Veneziano,[1] Iolanda Aquila,[1] Mariangela Scalise,[1] Teresa Mancuso,[1] Eleonora Cianflone,[1] Chiara Valeriano,[1] Pina Marotta,[1] Laura Tammè,[1] Carla Vicinanza,[1] Ferdinando C. Sasso,[4] Domenico Cozzolino,[4] Michele Torella,[5] Alessandro Weisz,[2] and Ciro Indolfi[1]

Diabetes 2018;67:2554–2568 | https://doi.org/10.2337/db17-1434

Harnessing the mechanisms underlying the exacerbated vascular remodeling in diabetes mellitus (DM) is pivotal to prevent the high toll of vascular diseases in patients with DM. miRNA regulates vascular smooth muscle cell (VSMC) phenotypic switch. However, miRNA modulation of the detrimental diabetic VSMC phenotype is underexplored. Streptozotocin-induced type 1 DM (T1DM) Wistar rats and type 2 DM (T2DM) Zucker rats underwent right carotid artery experimental angioplasty, and global miRNA/mRNA expression profiling was obtained by RNA sequencing (RNA-Seq). Two days after injury, a set of six miRNAs were found to be uniquely downregulated or upregulated in VSMCs both in T1DM and T2DM. Among these miRNAs, miR-29c and miR-204 were the most significantly misregulated in atherosclerotic plaques from patients with DM. miR-29c overexpression and miR-204 inhibition per se attenuated VSMC phenotypic switch in DM. Concomitant miR-29c overexpression and miR-204 inhibition fostered an additive reduction in VSMC proliferation. Epithelial membrane protein 2 (*Emp2*) and Caveolin-1 (*Cav1*) mRNAs were identified as direct targets of miR-29c and miR-204, respectively. Importantly, contemporary miR-29c overexpression and miR-204 inhibition in the injured artery robustly reduced arterial stenosis in DM rats. Thus, contemporaneous miR-29c activation and miR-204 inhibition in DM arterial tissues is necessary and sufficient to prevent the exaggerated VSMC growth upon injury.

Phenotypic switch of vascular smooth muscle cells (VSMCs) is a crucial event in the etiopathogenesis of vasculoproliferative diseases such as atherosclerosis, restenosis, and asthma (1–6). Diabetes mellitus (DM) exacerbates the synthetic/proliferative phenotype of VSMCs, which underlies the very high rate of vascular complications in patients with diabetes (7–9). Several key pathological factors associated with DM contribute to a particularly aggressive phenotypic switch of VSMCs in response to injury (10–12).

miRNAs have been implicated in several pathophysiological conditions including vasculoproliferative diseases (13–16). However, there is scant current knowledge about the role of miRNAs in VSMC dysfunction in diabetic vascular disease. Recently, it has been reported that DM misregulates miR-504, which promotes VSMC dysfunction in *db/db* mice with type 2 DM (T2DM) (17). However, it is likely that the detrimental diabetic phenotype of VSMCs in vasculoproliferative disease is mediated by multiple miRNAs whose contemporary dysregulation act together to alter the multifactorial vascular response in diabetes.

Using RNA sequencing (RNA-Seq) technology, here we identified a cluster of six differentially expressed miRNAs after vascular injury in rats with type 1 DM (T1DM) or T2DM. The latter were named vascular "Diab-miRs." Among these Diab-miRs, contemporary dysregulation of miR-29c and miR-204 was shown to be necessary and sufficient to determine the exaggerated proliferative phenotype of

[1]Cardiovascular Institute, Department of Medical and Surgical Sciences, Magna Graecia University, Catanzaro, Italy
[2]Laboratory of Molecular Medicine and Genomics, Department of Medicine, Surgery and Dentistry "Scuola Medica Salernitana," University of Salerno, Baronissi, Salerno, Italy
[3]Genomix4Life srl, Department of Medicine, Surgery and Dentistry "Scuola Medica Salernitana," University of Salerno, Baronissi, Salerno, Italy
[4]Department of Internal and Experimental Medicine "Magrassi-Lanzara," University of Campania "L. Vanvitelli," Naples, Italy
[5]Department of Cardiothoracic Sciences, University of Campania "L. Vanvitelli," Naples, Italy

Corresponding author: Daniele Torella, dtorella@unicz.it.

Received 10 December 2017 and accepted 14 September 2018.

This article contains Supplementary Data online at http://diabetes.diabetesjournals.org/lookup/suppl/doi:10.2337/db17-1434/-/DC1.

D.T. and C.Ia. equally contributed to this study.

VSMCs in DM. Indeed, local release of a bicistronic construct to simultaneously upregulate miR-29c and inhibit miR-204 prevented neointima formation after vascular injury in diabetic animals.

RESEARCH DESIGN AND METHODS

Animal Models

All animal experiments were performed under directive 2010/63/EU of the European Parliament and were approved by the Italian Ministry of Health. All rat strains were purchased from Charles River Laboratories. The study design is summarized in Supplementary Fig. 1*A*. To induce experimental T1DM, streptozotocin was injected intraperitoneally in male adult Wistar rats (18). As a model of T2DM, male obese inbred Zucker diabetic Fatty (ZDF) rats were used. Balloon injury of the right carotid artery was performed in rats, as previously described (13,18). Arterial stenosis (neointimal formation) was assessed at 14 days after balloon injury, as previously described (5,13,18).

RNA Sequencing

At 2 days after injury, total RNA was extracted from carotid arteries in each group and processed for RNA-Seq as previously described (19–23). Indexed libraries were prepared from 600 ng/each purified RNA pool with TruSeq Stranded Total RNA Sample Prep Kit (Illumina). Libraries were sequenced at a concentration of 10 pmol/L per lane on HiSeq1500 platform (Illumina). The raw sequence files generated underwent quality control analysis using FastQC (http://www.bioinformatics.babraham.ac.uk/projects/fastqc/), and the quality-checked reads were then aligned to the rat genome (rn4 assembly) using TopHat version 2.0.10.

Gene annotation was obtained for all known genes in the rat genome, as provided by Ensembl genome browser.

We calculated the number of reads mapping to each transcript with HTSeq-count. Raw read counts were then used as input to DESeq for the calculation of normalized signal for each transcript in the samples, and differential expression was reported as the fold change along with associated adjusted (Benjamini-Hochberg) *P* values. For small RNA-Seq, indexed libraries were prepared from 1 μg/each purified RNA pool. Sized indexed miRNA libraries were gel purified and sequenced in triplicate on a HiSeq1500 system (Illumina). The sequence data obtained were analyzed using the iSmart pipeline, using as reference miRBase version 18. Samples were technical quadruplicates. However, the single biological sample for each group refers to the pooling of RNA obtained from six carotid arteries from a corresponding number of animals. Functional and pathway analyses were performed using Ingenuity Pathway Analysis (IPA; Qiagen [www.ingenuity.com]).

Immunohistochemistry Analysis and Fluorescence In Situ Hybridization

For in vivo VSMC proliferation analysis, all animals received BrdU before sacrifice (13). At 2 days after injury, carotid arteries were embedded in paraffin and 5-μm cross sections were stained as previously reported (5,13). For the immunofluorescence detection of Epithelial Membrane Protein 2 (EMP2) and Caveolin 1 (CAV1), arterial sections were incubated with a rabbit monoclonal antibody against Cav1 (Cell Signaling Technology) and a rabbit polyclonal antibody against EMP2 (Bioss) and were revealed with appropriate anti-rabbit secondary antibody as per manufacturer instructions (5,13). VSMCs were detected using an antibody against α-smooth muscle actin (1:100; Sigma-Aldrich). The nuclei were counterstained with DAPI (Sigma-Aldrich). Fluorescence in situ hybridization of miR-29c and miR-204 was performed as previously described (13,24). Specific probes for mir-29c and miR-204 were from Qiagen (miRCURY LNA miRNA Detection Probe) and were revealed according to manufacturer instructions. All stainings were acquired and analyzed using confocal microscopy (TCS SP5 and SP8 microscopes; Leica).

In Vivo Analysis of miR-29c and miR-204

Adenovirus vectors encoding an siRNA for *Cav1* (Ad-si*Cav1*), miR-29c (Ad-miR-29c), and miR-204 inhibitor (Ad-miR-204-inhibitor) and their respective negative controls (NCs) were purchased from Applied Biological Materials. A bicistronic construct harboring miR-29c-mimic and miR-204-inhibitor was cloned in a standard adenoviral vector (Vector Biolabs). The adenovirus vector was named Adeno-Combo-miR-29c-m/miR-204-i (or Ad-29cM/204I). Adeno-Combo-negative mimic/inhibitor NC (for simplicity Ad-NC) was used as a control. Immediately after vascular injury, the balloon-dilated common carotid arteries were distally clumped to stop perfusion and were infused through the external carotid artery with the specific adenoviral constructs for 30 min (4×10^{10} plaque-forming units/mL). At the end, adenoviruses were retrieved from the external carotid arteries, the common carotid arteries were washed to ensure complete adenovirus removal, and then the distal clump was removed to allow the recovery of normal carotid perfusion (13). Animals were then sacrificed at 2 and 14 days. In separate experiments, miR-204-mimic and miR-29c-inhibitor were mixed with pluronic gel solution and were locally applied over the injured carotid artery (18).

Human Atherosclerotic Plaque Sample Collection

Human atherosclerotic plaques were derived from patients affected by symptomatic significant carotid artery lesions undergoing surgical carotid endarterectomy. Carotid endarterectomy was performed using standard techniques, with minor variations depending on surgeon and patient. After surgical removal, the specimen containing the plaque lesion was immediately flash frozen in liquid nitrogen and subsequently stored in liquid nitrogen until RNA extraction. Patients with T2DM and without diabetes (ND) were included in the study and did not differ significantly for any clinical parameter other than T2DM (Supplementary Table 1).

RNA Extraction and Real-time PCR Analysis

Total RNA was extracted with the TRIzol reagent or mirVana miRNA Isolation Kit (Invitrogen) (13). miRNA expression was evaluated using TaqMan miRNA assays (Applied Biosystems). TaqMan Gene Expression Assay (Applied Biosystems) was used for quantification of *Emp2*, *Cav1*, *Tagln*, and *Myh1* transcripts (15).

Cell Culture, Transfection, and Reagents

Primary rat aortic smooth muscle cells (SMCs) and human coronary artery SMCs were from Life Technologies. For gain-of-function and loss-of-function experiments, we used mimic and inhibitor RNA molecules purchased from Life Technologies. Cells were transfected using Lipofectamine RNAiMAX (Life Technologies). Specific ACCELL siRNAs against *Emp2* (siRNA/Emp2; Dharmacon) were used to inhibit *Emp2* mRNA expression in VSMCs. Cells were also transfected with *Emp2* Plasmid Vector [lacking *Emp2* 3′-untranslated region (UTR)] by Lipofectamine 2000 (Invitrogen).

Cell Proliferation Analysis

Proliferating VSMCs were identified using Click-it EdU (5-ethynyl-2′-deoxyuridine) kit (Invitrogen) for the detection of EdU incorporation into DNA. For cell cycle analysis, VSMCs were stained with propidium iodide (PI) using an FxCycle PI/RNAase Staining Solution Kit (Life Technologies). Flow cytometric analyses of the cell cycle were performed with FACSAria III (BD Biosciences).

Luciferase Reporter Assay

The wild type 3′ UTR of *Emp2* was cloned downstream of the Firefly/Renilla Duo-Luciferase reporter vector (GeneCopoeia Inc). HEK293 cells were transfected with *Emp2* 3′ UTR plasmid alone or cotransfected with miR-29c mimic. Luciferase activity was measured by Luc-Pair Luciferase Assay Kit (GeneCopoeia).

Western Blots and Immunoprecipitations

Western blotting and immunoprecipitation were performed by standard protocol as previously reported (5,13,18). The antibodies used were the following: mouse anti-CAV1 (sc-70516; Santa Cruz Biotechnology), goat anti-EMP2 (sc-132670; Santa Cruz Biotechnology), and mouse anti-GAPDH. Experiments were performed in biological quadruplicate, and the data are shown as the mean ± SD.

Statistics

Statistical analysis was performed with GraphPad Prism version 6.00 for Macintosh (GraphPad Software). Quantitative data are reported as the mean ± SD and binary data by counts. Significance between two groups was determined by Student *t* test or paired *t* test, as appropriate. For comparison between multiple groups, ANOVA was used. A P value <0.05 was considered significant. The Bonferroni post hoc method was used to locate the differences. In these cases, the type I error ($\alpha = 0.05$) was corrected by the number of statistical comparisons performed. For the in vitro cell and molecular biology experiments with an $n > 4$ sample size, giving the low number of the sample, the Kruskal-Wallis test (for multiple-group comparison), and the Mann-Whitney *U* test (for comparison between two groups) were performed.

RESULTS

Diabetes Exaggerates VSMC Proliferation and Neointima Formation After Balloon Injury

Balloon injury of the right common carotid artery was performed in T1DM male adult Wistar rats, T2DM ZDF rats (25), and in respective euglycemic controls (Supplementary Fig. 1*A*). At 2 days after injury, carotid arteries from both T1DM and T2DM animals showed a significantly increased VSMC proliferation rate when compared with controls (Fig. 1*A* and *B*). The increased VSMC proliferation rate was followed by a significant increase in neointima formation in injured carotid arteries from T1DM and T2DM rats (Fig. 1*C* and *D*).

Thus, both DM models reproduced previous findings (7,8,18) and confirmed that DM exaggerates the proliferative response of VSMCs in the media layer, increasing arterial narrowing at the site of vascular injury.

RNA-Seq Profiling of Vascular miRNA Signature in DM After Injury

Total RNA was extracted from injured and uninjured carotid arteries of each group and processed for small RNA-Seq as previously described (14). The bioinformatics analysis demonstrated the differential expression of >300 known miRNAs in each group. A read count cutoff of ≥100 in at least one replicate was established. After this correction, the bioinformatics analysis covered >70 miRNAs for each group (Supplementary Tables 2–4). A heat map of global differentially expressed miRNAs is shown in Fig. 2*A*. Heat map visualization of miRNA expression values between uninjured and injured vessels from each group is provided in Supplementary Fig. 1*B*. Different miRNAs already proven to be involved with the proliferative phenotype of VSMCs were accordingly upregulated or downregulated after balloon injury in euglycemic control rats. The latter confirms previous reports (13,26,27) and shows that the approach used can reliably assess the question posed with this experimental design.

The Venn diagram in Fig. 2 summarizes the number and overlap of upregulated (Fig. 2*B*) and downregulated (Fig. 2*C*) miRNAs in the injured arteries of the three groups. The analysis revealed significant differences in the dysregulated miRNAs among the experimental groups. We then filtered the list of miRNAs showing a differential expression in at least one group with an arbitrary fold change ≥1.5 and an adjusted P value false discovery rate (FDR) <0.05. Based on these parameters, we observed the abundance of significantly deregulated miRNAs in each group (Fig. 2*D*–*F*). Thirty-six miRNAs were identified as being robustly differentially expressed in injured arteries in euglycemic rats, 47 miRNAs in T1DM rats, and 38 miRNAs in T2DM rats.

The Volcano plots representing the dysregulated miRNAs in injured versus uninjured arteries revealed that a few miRNAs were specifically upregulated or downregulated in both T1DM and T2DM rats but not in euglycemic rats (Fig. 2*G–I*). In particular, miR-195, miR-29c, miR-140-3p, and miR-199a-5p were downregulated in both T1DM and T2DM, while miR-25 and miR-204 were, on the other hand, specifically upregulated in both DM types. Thus, these six miRNAs (Diab-miRs), potentially constitute a diabetic signature underlying/regulating the proliferative response of VSMCs in DM.

Diabetic miRNA Signature Is Conserved in Human Atherosclerotic Plaques

Interestingly, the fold changes of all selected miRNAs as determined by quantitative RT-PCR (qRT-PCR) strongly correlated with the values from the RNA-Seq (Fig. 3*A*).

Among the four downregulated Diab-miRs, mir-29c downregulation by a miR-29c-inhibitor shows the more pronounced increase in VSMC proliferation in low-serum conditions. Concurrently, miR-204 upregulation increased VSMC proliferation (Fig. 3*B*).

We then compared expression levels of the six identified miRNAs in human atherosclerotic plaque specimens from age- and sex-matched patients with diabetes and nonpatients with diabetes undergoing surgical carotid endarterectomy for symptomatic carotid artery stenosis. We found that miR-195, miR-29c, and miR-199a-5p were all downregulated while miR-204 was upregulated in diabetic versus ND samples (Fig. 3*C*).

Among the dysregulated miRNAs, considering their functional preliminary evaluation in vitro and their expression profile in human vascular tissues, mir-29c and miR-204 appeared to have the highest potential to specifically regulate diabetes-dependent VSMC hyperplastic phenotype. The latter is further reinforced by the absence of miR-29c and miR-204 dysregulation in peripheral blood monocytes and T cells from T1DM, T2DM, and euglycemic control rats 2 days after injury (Supplementary Fig. 2*A–C*). This further suggests that diabetes-induced dysregulation of miR-29c and miR-204 primarily involves VSMCs without targeting other cell types known to contribute to pathological arterial narrowing.

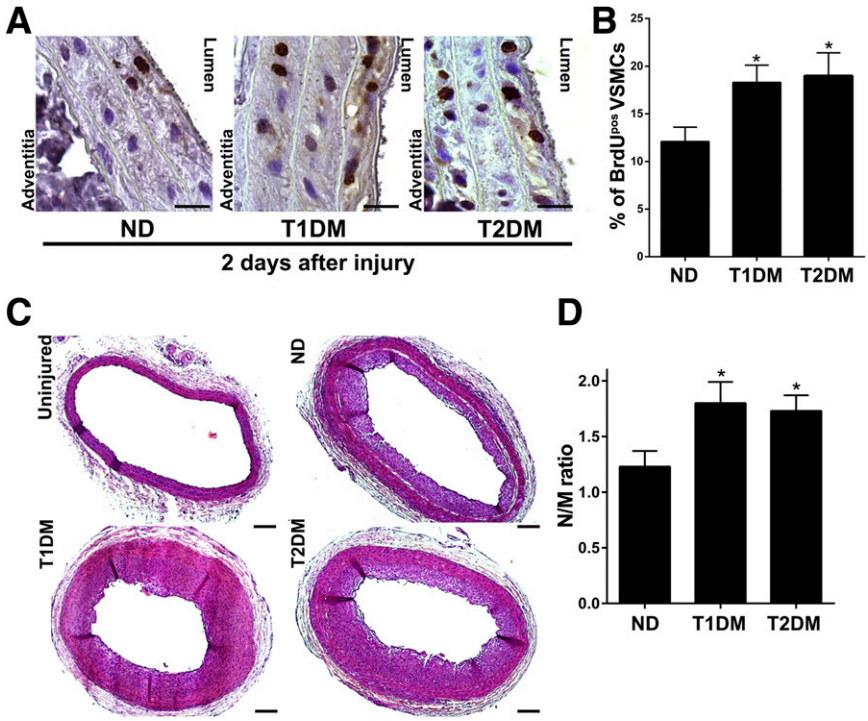

Figure 1—Effects of diabetes on VSMC proliferation and neointima formation after balloon injury. *A*: Representative histological images of diaminobenzidine immunohistochemical staining for BrdU-positive (dark brown) VSMC nuclei in the media layer of injured carotid arteries from control euglycemic Wistar (ND), T1DM, and T2DM rats 2 days after injury. Scale bar = 20 μm. *B*: Quantification of medial VSMC proliferation at 2 days after injury. *$P < 0.05$ vs. control euglycemic rats (ND). *C*: Representative hematoxylin-eosin (H-E) staining of carotid cross sections 14 days after balloon injury from ND (top right panel), T1DM (bottom left panel), and T2DM (bottom right panel) groups. For direct comparison, representative image of an uninjured carotid artery is shown in the top left panel. Scale bar = 100 μm. *D*: Bar graph shows cumulative data of arterial stenosis formation (neointima formation) in the study groups, as measured by the morphometric analysis of H-E–stained sections of injured carotid arteries reported as the ratio between the areas of media and neointima layers 14 days after balloon damage. *$P < 0.05$ compared with the ND group. Data are presented as the mean ± SD. To simplify the data presentation, the values for ND Zucker lean rats are not presented as they have a vascular response to injury that is practically indistinguishable from that of Wistar rats (data not shown).

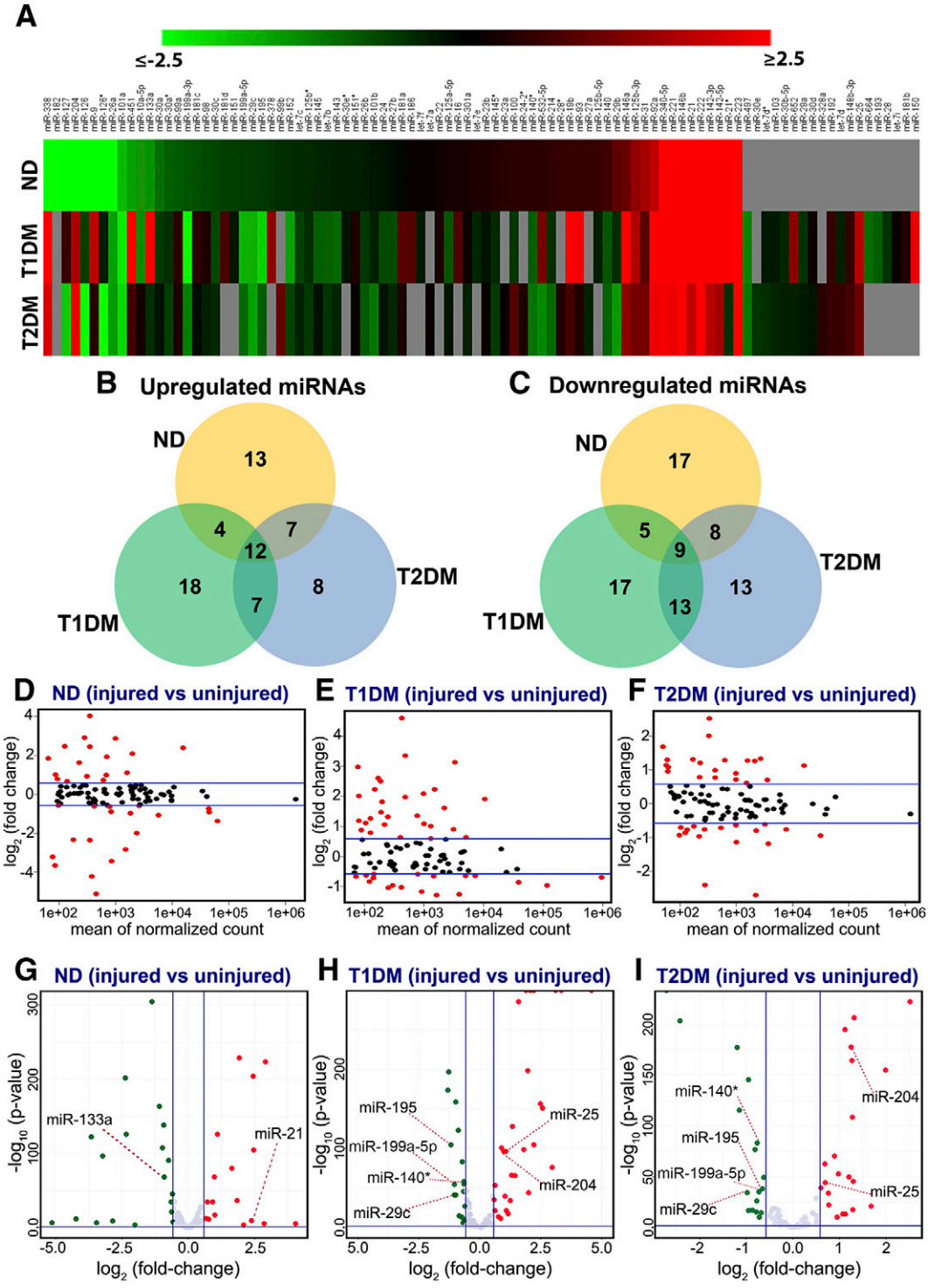

Figure 2—Expression analysis of vascular miRNAs by RNA-Seq 2 days after injury. *A*: Representative heat map of differentially expressed miRNAs based on small RNA-Seq results. Fold change (cutoff |1.5|; FDR ≤0.05) in miRNA expression at 2 days after vascular injury was used to plot the heat map. Average values obtained from three independent technical replicate samples are reported. An arbitrary cutoff of normalized read count (≥100) was also used to filter the small RNA-Seq data. *B* and *C*: Venn diagrams of upregulated and downregulated miRNAs in the injured arteries from ND, T1DM, and T2DM rats. *D*, *E*, and *F*: M-A plot (scatter plot of log2-fold change [M variable] versus mean between the intensity values [A variable]) of differentially expressed miRNAs (fold change ≥1.5) in injured arteries from ND (*D*), T1DM (*E*), and T2DM (*F*) carotid arteries compared with the respective uninjured carotid arteries. Red dots represent the significant differentially expressed miRNAs (cutoff ≥100) with an adjusted *P* value (FDR) <0.05. *G*, *H*, and *I*: Volcano plot analysis of differentially expressed miRNAs in the injured vs. uninjured carotid arteries from ND (*G*), T1DM (*H*), and T2DM (*I*) rats. Log2 transformation of the fold change in miRNA expression between injured and uninjured arteries from each group is plotted on the *x*-axis. The log FDR-adjusted *P* value (base 10) is placed on *y*-axis. Differentially expressed miRNAs (fold change ≥1.5) are indicated in red (upregulated miRNAs in injured vs. uninjured) and in green (downregulated miRNAs in injured vs. uninjured). miR-140*, miR-140-3p.

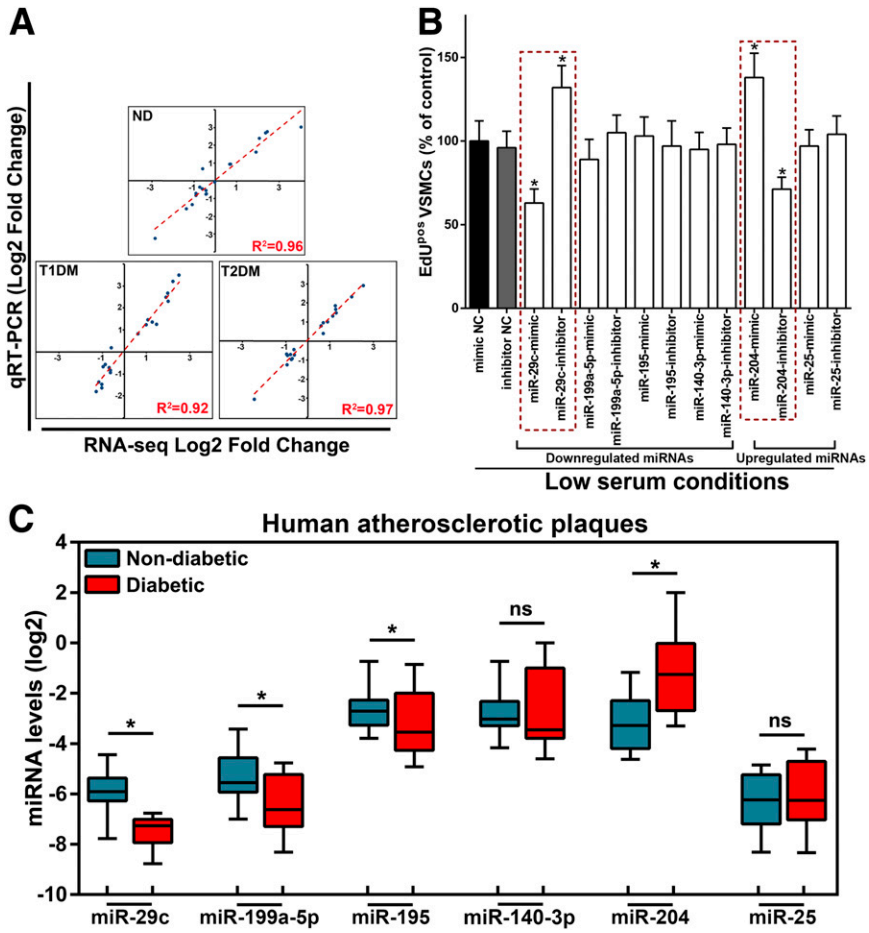

Figure 3—qRT-PCR analysis of the differentially expressed Diab-miRs. *A*: qRT-PCR validation of the six RNA-Seq–selected differentially expressed Diab-miRNAs (miR-29c, miR-199a-5p, miR-195, miR-140-3p, miR-204, and miR-25) and of additional RNA-Seq–assessed differentially expressed random miRNAs in the injured arteries from ND, T1DM, and T2DM carotid arteries vs. the respective uninjured carotid arteries. Real-time PCR was performed using TaqMan miRNA assays. U6 RNA was used as the internal control for data normalization. Log2 transformation of the fold changes from RNA-Seq results is plotted on the *x*-axis. Log2 ratios from qRT-PCR are placed on the *y*-axis. R^2 represents the correlation coefficient. *B*: Cumulative data of the effects of gain-of-function and loss-of-function of the six Diab-miRs on VSMC proliferation (as measured by EdU incorporation) in vitro in low-serum (2%) culture media. Bar graphs show the percentage of EdU-positive VSMCs transfected with the respective Diab-miR mimic or inhibitor compared with control scrambled mimic or inhibitor. *$P < 0.05$ vs. VSMC transfected with mimic or inhibitor NC, respectively. $N = 4$/group. Data are presented as the mean ± SD. *C*: qRT-PCR analysis of the differentially expressed Diab-miRs in atherosclerotic plaque from carotid atherectomy of subjects with and without diabetes. Data are presented as a box plot where all fold changes were calculated between medians. The y-axis indicates expression levels of Diab-miRs on a log2 scale. All *P* values were determined by the nonparametric Mann-Whitney *U* test. *$P < 0.05$ vs. miRNA expression in plaque of ND subjects. NS, not significant.

miR-29c and miR-204 Regulation of VSMC Phenotypic Switch

Rat aortic VSMCs were treated with high glucose (HG; 25 mmol/L) and high insulin (HI; 200 nmol/L) as DM conditions in vitro. Control cells were cultured in normal (low) glucose (5 mmol/L) and insulin (2 nmol/L). miR-29c was downregulated, while miR-204 was upregulated in HI/HG conditions (Supplementary Fig. 3*A*). Similar effects were also detected in human coronary artery SMCs (Supplementary Fig. 3*B*).

A standard model of the VSMC phenotypic switch in vitro involves the treatment of VSMCs with platelet-derived growth factor (PDGF)-BB (28,29). VSMCs were transfected with miR-29c and miR-204 mimics or inhibitors to test whether PDGF-BB–dependent VSMC proliferation in HG conditions is modulated by these miRNAs. miR-29c overexpression or miR-204 inhibition in PDGF-BB+HG–treated VSMCs caused a significant decrease in proliferating cells when compared with the relative specific controls, whereas the opposite effect was obtained with the inhibition of miR-29c or miR-204 overexpression, respectively (Fig. 4*A*).

The VSMC phenotypic switch commences with cell dedifferentiation through the downregulation of VSMC contractile genes (13). We then analyzed the effects of miR-29c and miR-204 gain-of-function or loss-of-function on the expression of Transgelin (*Tagln*) and Myosin Heavy Chain 11 (*Myh11*) in PDGF-BB+HG–treated VSMCs. These two genes are indeed specifically expressed by contractile VSMCs, and their downregulation is classically related to

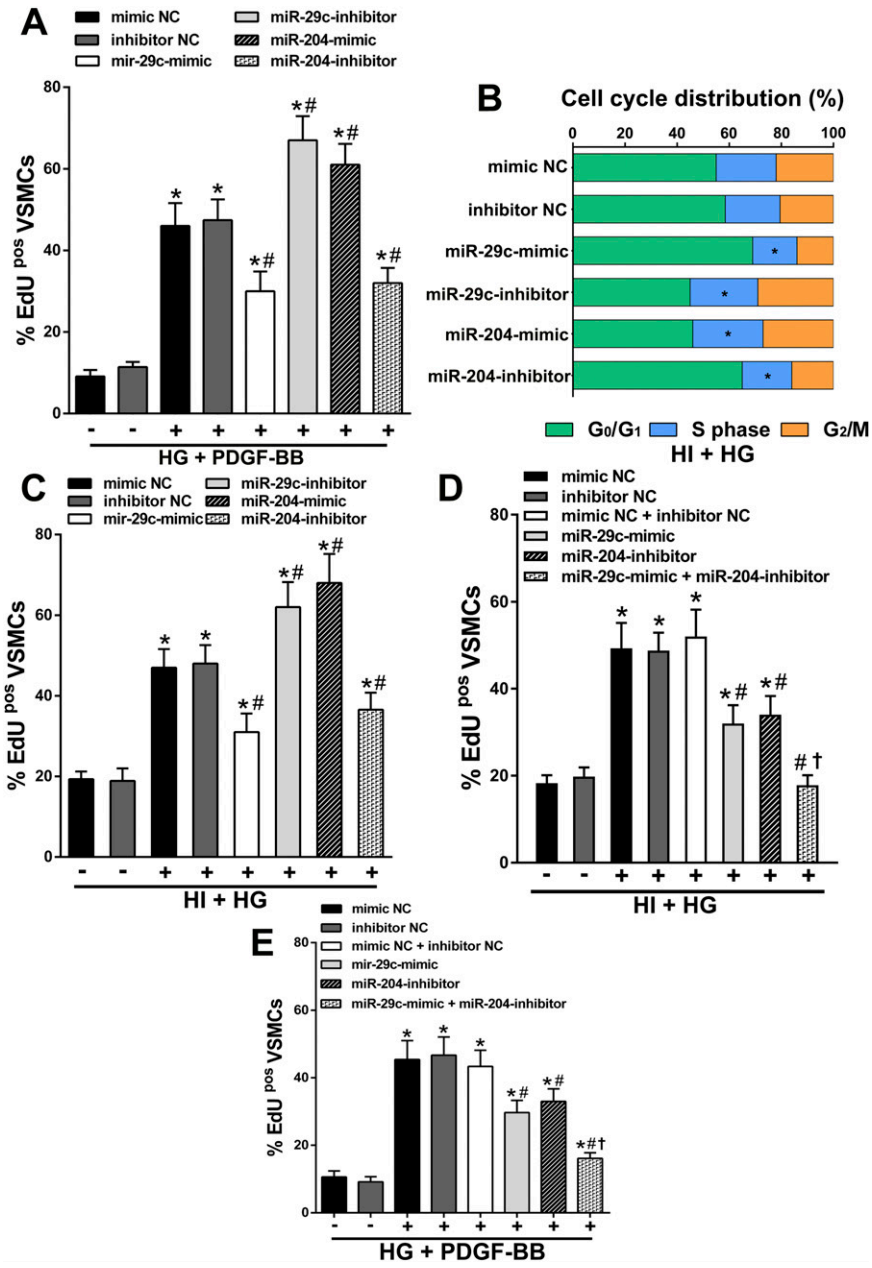

Figure 4—Effects of miR-29c and miR-204 modulation on VSMC proliferation in vitro. *A*: Percentage of proliferating (EdU^{pos}) cells in 48-h HG + PDGF-BB–stimulated VSMCs transfected with miR-29c-mimic, miR-29c-inhibitor, miR-204-mimic, miR-204-inhibitor, and mimic or inhibitor NC (Note: mannitol [25 mmol/L] was used as a further control of glucose concentrations in vitro; mannitol did not affect VSMC proliferation when compared with normal [low] glucose [data not shown]). *$P < 0.01$ vs. unstimulated cells transfected with mimic or inhibitor NC. #$P < 0.01$ vs. HG/PDGF-stimulated VSMCs transfected with NC. $N = 4$/group. *B*: Effects of miR-29c and miR-204 modulation on cell cycle progression. VSMCs were transfected with mimic NC, inhibitor NC, miR-29c-mimic, miR-29c-inhibitor, miR-204-mimic, or miR-204-inhibitor and stimulated with HG and HI. Cell cycle profiles were determined by PI staining and flow cytometry analysis. Bar graphs represent the percentages of cells in the G_0/G_1, S, and G_2/M phases of the cell cycle. *$P < 0.01$ vs. VSMCs transfected with mimic or inhibitor NC. $N = 4$. *C*: Percentage of proliferating cells (EdU incorporation) in unstimulated and HG/HI-stimulated VSMCs transfected with mimic NC, inhibitor NC, miR-29c-mimic, miR-29c-inhibitor, miR-204-mimic, or miR-204-inhibitor. *$P < 0.01$ vs. unstimulated cells transfected with mimic or inhibitor NC. #$P < 0.01$ vs. HG/HI-stimulated VSMCs transfected with mimic or inhibitor NC. $N = 5$. *D*: Bar graphs represent the percentages of EdU-positive cells in unstimulated and HG/HI-stimulated VSMCs upon transfection with either a combination of miR-29c-mimic and miR-204-inhibitor or each RNA molecule alone. *$P < 0.01$ vs. unstimulated VSMCs transfected with NC. #$P < 0.01$ vs. HG/HI-stimulated VSMCs transfected with NC. †$P < 0.01$ compared with VSMCs transfected with miR-29c-mimic. $N = 5$. *E*: Bar graphs represent the percentages of EdU-positive cells in PDGF-BB–stimulated and HG-stimulated VSMCs upon transfection with miR-29c-mimic, miR-204-inhibitor, or the combination of both miR-29c-mimic and miR-204-inhibitor. *$P < 0.01$ vs. unstimulated VSMCs transfected with NC. #$P < 0.01$ vs. stimulated VSMCs transfected with relative controls. †$P < 0.01$ compared with VSMCs transfected with miR-29c-mimic. $N = 5$. Data are presented as the mean ± SD.

the phenotypic switch of VSMCs underlying vasculoproliferative disorders (13,15). miR-29c overexpression partially inhibited while miR-29c inhibition exacerbated PDGF-BB–induced *Tagln* and *Myh11* downregulation in HG conditions (Supplementary Fig. 3*C*). A significant decrease in *Tagln* and *Myh11* was also observed in the VSMCs transfected with miR-204 mimic compared with the control group (Supplementary Fig. 3*D*). The opposite effect was elicited by miR-204 downregulation.

Furthermore, miR-29c-mimic or miR-204 inhibitor reduced HI/HG-stimulated VSMCs in the S phase of the cell cycle compared with cells transfected with relative controls (Fig. 4*B*). On the contrary, miR-204 overexpression or miR-29c inhibition increased the number of VSMCs in S phase (Fig. 4*B*).

miR-29c overexpression or miR-204 inhibition causes a significant decrease in EdU^+ proliferating VSMCs in response to HI/HG conditions (Fig. 4*C*). Accordingly, miR-29c inhibition or miR-204 mimic fostered a significant increase in EdU incorporation in HI+HG-stimulated VSMCs. Notably, concomitant miR-29c overexpression and miR-204 inhibition had an additive effect when compared with the single miRNA modulation in reducing HI/HG-induced VSMC proliferation (Fig. 4*D*). Finally, simultaneous miR-29c upregulation and miR-204 downregulation increased the cell cycle inhibition of PDGF-BB+HG–stimulated VSMCs when compared with unstimulated VSMCs and VSMCs treated with either miR-29c-mimic or miR-204 inhibitor (Fig. 4*E*).

Thus, these data collectively show that miR-29c and miR-204 additively modulate the hyperproliferative phenotype of VSMCs in diabetic conditions in vitro.

Diabetes Differently Regulates Vascular Transcriptome Upon Injury

Whole transcriptome analysis was performed on the same RNA extracted for miRNome analysis from uninjured and injured carotid arteries of T1DM, T2DM, and euglycemic rats 2 days after injury (23). Several mRNAs were differentially expressed (read count cutoff >10 in at least one replicate) using the normalized reads showing a >1.5-fold change in injured carotid arteries compared with the uninjured control group. We found 2,210 upregulated and 2,469 downregulated genes in injured versus uninjured carotid arteries from T1DM rats and 1,494 upregulated and 2,246 downregulated genes in injured versus uninjured carotid arteries from T2DM rats. Functional analysis of differentially expressed mRNAs through IPA indicated that several pathways related to VSMC phenotypic switch were activated in both DM models (Fig. 5*A*). Disease and function analyses identified by IPA also indicated that the highest fraction of dysregulated genes in both T1DM and T2DM cluster in gene ontologies involved with cell proliferation, RNA processing, cell apoptosis, cell migration, and metabolism (Fig. 5*B*).

Dysregulated mRNAs in injured versus uninjured carotid arteries were searched to identify all of the putative miR-29c and miR-204 mRNA targets whose changes were specular to the relative miRNA modulation. miRanda analysis shows that of the 477 mRNA targets of miR-29c, 88 were upregulated in T1DM rats and 58 in T2DM rats. Concurrently, of the 597 putative mRNA targets of miR-204, 123 were downregulated in T1DM rats and 108 in T2DM rats. Then, we restricted the analysis on dysregulated genes that had a fold change of less than or equal to -1.5 or ≥ 1.5 ($|1.5|$) and that were present in both T1DM and T2DM rats but not in the euglycemic controls or that were significantly more upregulated or downregulated in both T1DM and T2DM rats versus euglycemic controls. The heat map of differentially expressed mRNAs in each group is shown in Fig. 5*C* and *D*.

Of note, among the small set of putative miR-29c and miR-204 targets, IPA analysis revealed enrichment in specific signaling and metabolic pathways involved in VSMC phenotypic switch and vascular disorders (Supplementary Fig. 4*A* and *B*). The miRNA-mRNA target deregulated in both DM models included molecules implicated in cell cycle regulation, cell death, morphology, and migration (Supplementary Fig. 5*A* and *B*).

Overall, the bioinformatics analysis suggested that miR-29c and miR-204 coherently target relevant mRNAs underlying VSMC hyperplastic phenotype.

mRNA Targets of miR-29c Modulating VSMC Phenotype

Putative targets of miR-29c were further screened for their role on various biological processes potentially involved in the VSMC phenotypic switch regulation. We identified *Dclk1* (Doublecortin-Like Kinase 1), *Tnfrsf12a* (TNF Receptor Superfamily Member 12A), and *Emp2* as being among the top nine candidate transcripts identified. RT-PCR analysis revealed no significant differences in *Dclk1* and *Tnfrsf12a* expression in miR-29c-mimic–transfected or miR29c-inhibitor–transfected VSMCs (Supplementary Fig. 6*A*). Importantly, miR-29c-mimic significantly inhibited the expression of *Emp2* mRNA, whereas the opposite effect was obtained with the miR-29c-inhibitor (Fig. 6*A*). Since *Emp2* is a key element for different cell functions such as proliferation, migration, and cell adhesion (30,31), we next aimed to assess whether *Emp2* plays a role in the miR-29c regulation of VSMCs proliferation.

Consistent with the in vivo data, we first observed that EMP2 protein expression was increased in response to HI/HG conditions compared with VSMCs cultured in normal glucose and insulin (Fig. 6*B*). EMP2 protein decreased in VSMCs transfected with miR-29c-mimic and its specular increase in miR-29c-inhibitor–treated VSMCs (Fig. 6*B*). Ago proteins-RNA immunoprecipitation assay revealed that *Emp2* mRNA was significantly enriched in the Ago-immunoprecipitated RNAs from SMCs transfected with miR-29c-mimic compared with those treated with mimic NC (Supplementary Fig. 6*B*). On the contrary, *Emp2* mRNA significantly decreased in the Ago-immunoprecipitated RNAs from miR-29c-inhibitor–treated SMCs compared with cells

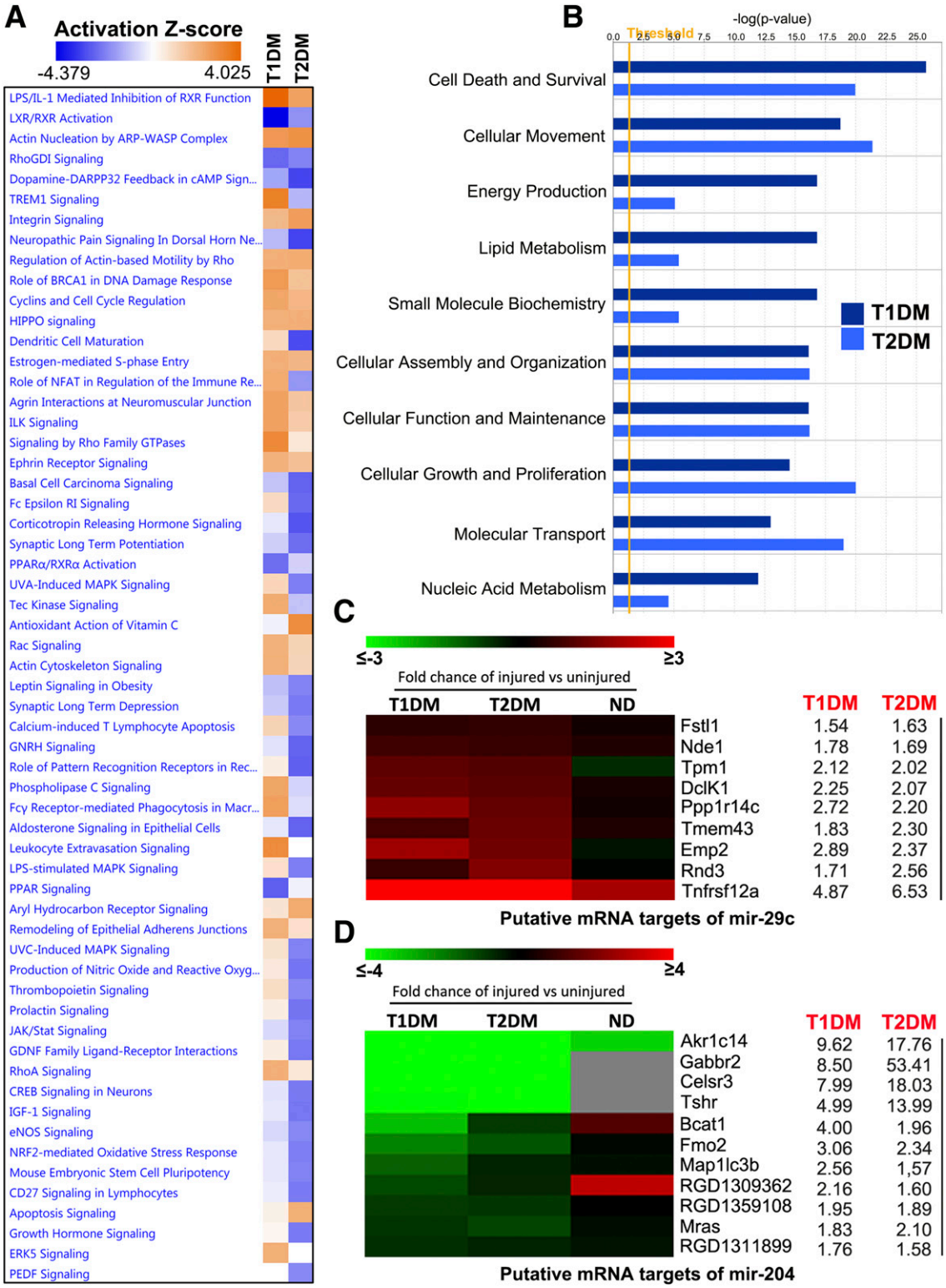

Figure 5— Differential expression analysis of mRNAs by RNA-Seq in injured carotid arteries of diabetic rats. *A*: Heat map, showing the most affected canonical molecular pathways, was generated by IPA of differentially expressed mRNAs from injured vs. uninjured arteries of T1DM and T2DM rats 2 days after balloon damage. Pathways are ranked according to the activation *z* score. Activated canonical pathways are indicated in orange. Blue indicates negative *z* score, representing putatively inhibited pathways. *B*: Disease and function analysis of the upregulated and downregulated mRNAs in injured arteries from T1DM and T2DM rats. *P* value (presented in −log10) >1.3. *C* and *D*: Heat maps of putative miR-29c and putative miR-204 target mRNAs based on RNA-Seq results. Differentially expressed (fold change |1.5|; cutoff >10) mRNAs at 2 days after vascular injury was used to plot the heat maps.

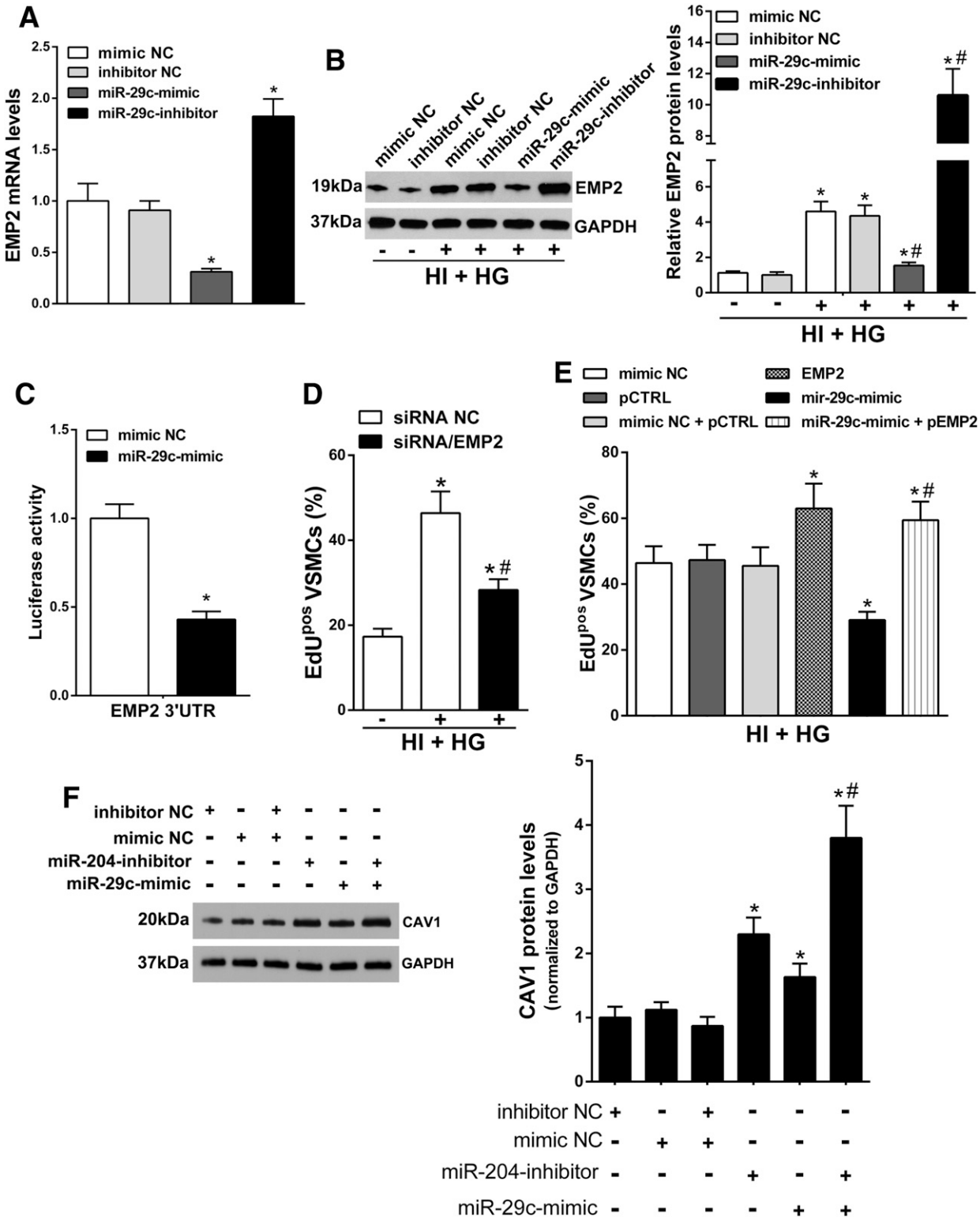

Figure 6— mRNA targets of miR-29c and miR-204 modulating VSMC proliferation. *A*: VSMCs were transfected with mimic NC, inhibitor NC, miR-29c-mimic, or miR-29-inhibitor. Emp2 expression was determined by qRT-PCR analysis. GAPDH was used as the internal control. *$P <$ 0.01 compared with all. $N = 4$/group. *B*: Representative immunoblotting (left) and cumulative quantification (right) of Emp2 protein levels in VSMCs transfected with miR-29c-mimic, miR-29c-inhibitor, mimic NC, or inhibitor NC. *$P < 0.01$ vs. control (VSMCs cultured in normal glucose and insulin). #$P < 0.01$ vs. HI/HG-stimulated VSMC transfected with NC. $N = 5$/group. *C*: Bar graphs represent the luciferase activity in HEK293 cells transfected with wild-type Emp2 3′ UTR target sequence expression plasmid and mimic-NC or miR-29c-mimic respectively. *$P < 0.05$ vs. control. $N = 4$. *D*: Percentage of proliferating cells in HI/HG-stimulated VSMCs transfected with siRNA/Emp2 or siRNA NC. *$P <$ 0.01 vs. siRNA NC-transfected VSMCs cultured in normal/low glucose and insulin. #$P < 0.05$ vs. HI/HG-stimulated VSMCs transfected with SiRNA NC. $N = 4$. *E*: VSMCs were cotransfected with the pEMP2 and miR-29c-mimic. Bar graphs represent the percentage of EdU-positive

transfected with inhibitor NC (Supplementary Fig. 6*B*). Accordingly, miR-29c-mimic reduced luciferase activity of a *Emp2* 3′ UTR cloned into a luciferase reporter construct transfected in HEK293 cells, showing that this miRNA directly targets *Emp2* 3′ UTR (Fig. 6*C*).

Finally, siRNA/*Emp2* significantly decreased VSMC proliferation in response to HI/HG conditions in vitro (Fig. 6*D* and Supplementary Fig. 6*C*). EdU incorporation assay was also performed in VSMCs cotransfected with plasmids encoding for *Emp2* (pEMP2) and miR-29c-mimic. p*Emp2* overexpression increased proliferating VSMCs despite miR-29c upregulation when compared with cells cotransfected with a NC plasmid and miR-29c-mimic (Fig. 6*E*).

Hence, overall these data show that miR-29c directly represses *Emp2*, which is a main target modulating miR-29c regulation of VSMC proliferation.

miR-204 Targets CAV1 in VSMC

We searched cellular and molecular functions of all putative miR-204 targets identified by RNA-Seq and in silico analysis. However, we did not identify any targets potentially involved with the hyperproliferative VSMC phenotype in the annotated mRNAs in injured arteries.

We thus evaluated the expression of CAV1 protein, a known target of miR-204 for its potential role in modulating VSMC proliferation (32,33). Accordingly, *Emp2* was previously shown to negatively regulate *Cav1* expression (34,35). Importantly, miR-204 directly affects CAV1 protein, but shows very limited effects on its mRNA expression (36). First, Ago-RNA immunoprecipitation assays show that *Cav1* mRNA was significantly enriched in the Ago-immunoprecipitated RNAs from the miR-204–overexpressing SMCs compared with the relative control, confirming that *Cav1* is a direct target of miR-204 (Supplementary Fig. 6*D*). Second, *Cav1* protein was significantly decreased in HI+HG–treated versus control VSMCs (Supplementary Fig. 6*E*). Importantly, miR-204 overexpression significantly inhibited CAV1 protein expression, whereas the opposite effect was obtained through functional inhibition of miR-204 (Supplementary Fig. 6*E*).

Furthermore, CAV1 protein expression was reduced by *Emp2* plasmid overexpression (Supplementary Fig. 6*F*), whereas siRNA-*Emp2* significantly increased CAV1 protein levels in VSMCs (Supplementary Fig. 6*G*). Finally, we assessed whether CAV1 protein levels could be modulated by concomitant miR-29c overexpression and miR-204 inhibition. VSMCs transfected with miR-29c-mimic or miR-204-inhibitor showed significantly increased CAV1 levels when compared with relative control cells (Fig. 6*F*). Interestingly, CAV1 protein expression was further induced by the combination of miR-204 downregulation and miR-29c upregulation (Fig. 6*F*).

These findings show that miR-204 fine-tunes CAV1 protein expression. This regulation links miR-204 and miR-29c activities, as they both converge to target *Cav1* in the molecular network activating VSMC proliferation.

An Adenoviral-Carried Bicistronic miR-29-Mimic and miR-204-Inhibitor Construct Abolishes VSMC Phenotypic Switch After Balloon Injury in Diabetic Rats

We assessed arterial stenosis formation (neointimal formation) in balloon-injured arteries from T1DM and T2DM rats infected with Ad-miR-29c or Ad-miR-204-inhibitor. Balloon-injured vessels showed reduced miR-204 levels 48 h after infection with Ad-miR-204-inhibitor, whereas Ad-miR-29c infection increased vascular miR-29c levels (Supplementary Fig. 7*A*). Concurrently, Ad-miR-29c significantly inhibited vascular *Emp2* mRNA expression (Supplementary Fig. 7*B*), whereas CAV1 protein levels were upregulated by Ad-miR-204-inhibitor (Supplementary Fig. 7*C*). Neointimal formation (measured as Neointima-media areas ratio) in injured vessels infected with Ad-miR-29c or Ad-miR-204-inhibitor were both decreased at 14 days compared with the control Ad-NC–treated injured vessels in T1DM and T2DM rats (Supplementary Fig. 7*D*). However, these two miRNA modulators separately did not decrease neointima formation beyond the vessel response to injury in euglycemic rats (Supplementary Fig. 7*D*).

We therefore designed a bicistronic construct to contemporarily overexpress miR-29c and antagonize miR-204. This bicistronic construct was cloned in an adenoviral vector for in vivo administration. The Adeno-Combo-miR-29c-*m*/miR204-*i* (or Ad-29cM/204I) was preliminarily tested in vitro, showing its effectiveness in inhibiting VSMC proliferation (Supplementary Fig. 7*E*). Ad-29cM/204I was locally released in injured carotid arteries from T1DM and T2DM rats where it increased vascular miR-29c levels and reduced miR-204 levels 2 days after balloon injury both in T1DM and T2DM rats when compared with the respective controls (Supplementary Fig. 8*A*). Fluorescence in situ hybridization showed that at 2 days after injury, miR-29c was downregulated, whereas EMP2 was upregulated specifically in VSMCs of injured carotid arteries from T2DM rats when compared with uninjured controls (Fig. 7*A*). miR-204 in situ levels were barely detectable in VSMCs of the media layer of uninjured arteries; however, miR-204 levels significantly increased in the VSMCs of balloon-injured carotid arteries, whereas

cells for each group. *$P < 0.05$ vs. VSMCs transfected with mimic NC. #$P < 0.05$ vs. VSMCs transfected with miR-29c-mimic. $N = 4$. *F*: Representative immunoblotting (left) and quantification (right) of Cav1 protein levels in VSMCs transfected with mimic NC, inhibitor NC, miR-29-c-mimic, miR-204-inhibitor, or combined miR-204-inhibitor and miR-29c-mimic. *$P < 0.05$ vs. control. #$P < 0.05$ vs. VSMCs transfected with miR-29c-mimic or miR-204-inhibitor. $N = 4$. Data are presented as the mean ± SD. pCTRL, plasmid control.

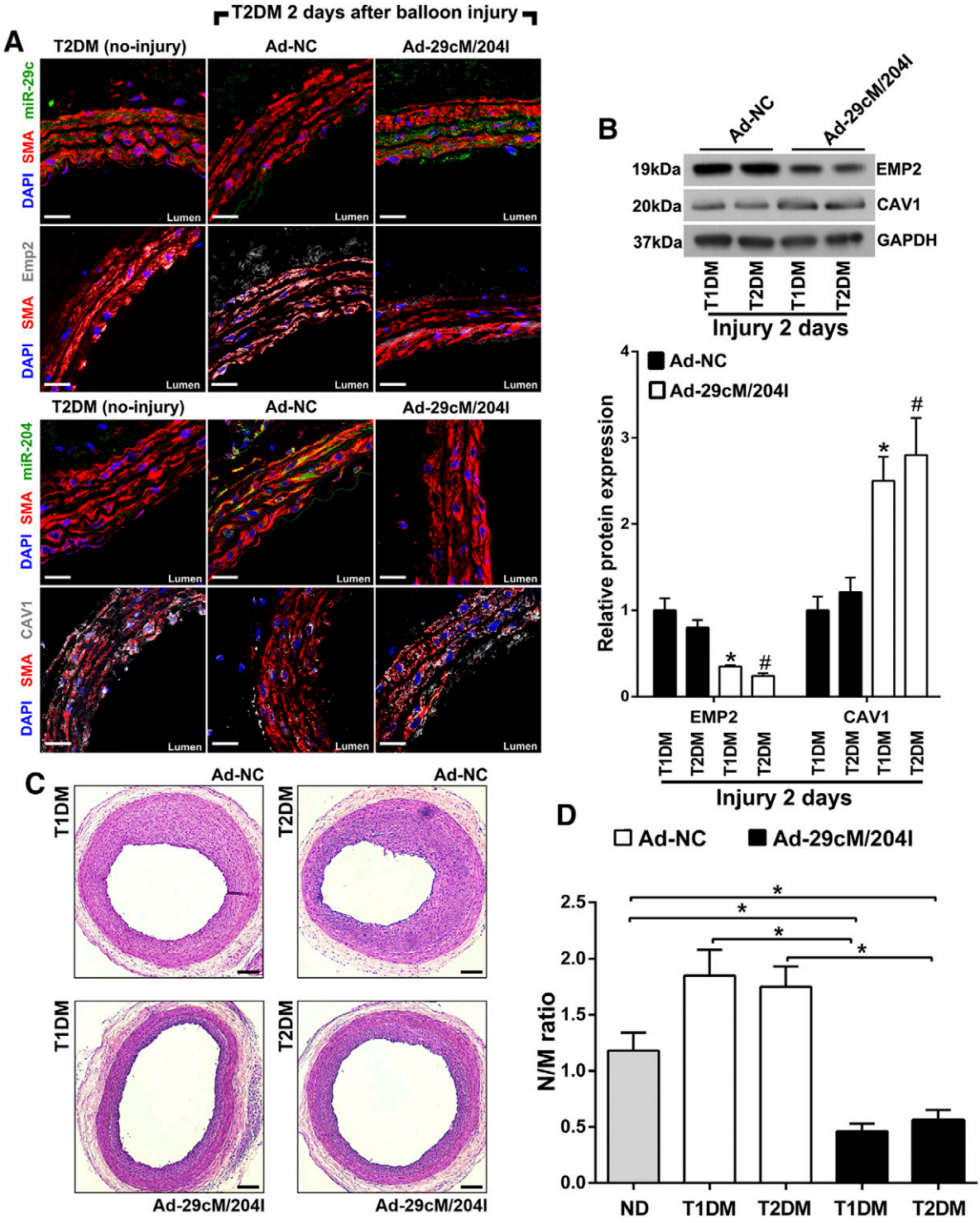

Figure 7—Concomitant overexpression of miR-29c and miR-204 inhibition prevents arterial stenosis formation after balloon injury in diabetic rats. *A*: In situ detection of miR-29c and miR-204 with concomitant EMP2 and CAV1 expression in T2DM rat carotid arteries treated with Ad-29cM/204I or Ad-NC (2 days after balloon injury). DAPI (blue) depicts cell nuclei; red fluorescence shows α-smooth muscle actin (SMA) staining; green indicates miR-204 or miR-29c; white indicates EMP2 or CAV1. Scale bar = 15 μm. *N* = 5/group. *B*: Emp2 and Cav1 expression (representative immunoblotting [top panel] and quantification [bottom panel]) in injured carotid arteries from T1DM and T2DM rats treated with Ad-29cM/204I compared with Ad-NC–treated vessels. **P* < 0.05 vs. injured artery from T1DM rats infected with Ad-NC. #*P* < 0.05 vs. injured artery from T2DM rats infected with Ad-NC. *N* = 6/group. *C*: Representative hematoxylin-eosin staining of carotid cross sections 14 days after balloon injury from the different group of animals included in the Ad-29cM/204I in vivo study. Ad-NC–treated rats (T1DM, top left panel; T2DM, top right panel) were used as controls. *N* = 6/group. *D*: Bar graph shows cumulative morphometric analysis of arterial stenosis represented by neointima formation (N/M areas ratio) in carotid arterial sections from the different group of animals included in the Ad-29cM/204I in vivo study. **P* < 0.05 compared with the Ad-NC–treated rats or ND euglycemic Wistar rats. *N* = 6/group. Data are presented as the mean ± SD.

CAV1 showed a specular decrease (Fig. 7*A*). Finally, Ad-29cM/204I infection respectively increased miR-29c while it decreased miR-204 levels specifically in VSMCs of balloon-injured carotid arteries (Fig. 7*A*). On the contrary, Ad-29cM/204I transduction reduced VSMC EMP2 levels while it increased CAV1 (Fig. 7*A*). Western blot analysis confirmed that vascular EMP2 protein levels were downregulated while CAV1 was upregulated in injured carotid arteries from T1DM and T2DM rats treated with Ad-29cM/204I compared with relative controls (Fig. 7*B*). Fourteen days after injury, miR-29c and miR-204 levels were, respectively, persistently upregulated and downregulated in Ad-29cM/204I–treated vessels when compared with injured controls (Supplementary Fig. 8*B*). Specular yet consistent data were obtained evaluating EMP2 and CAV1 levels in the injured carotid arteries at 14 days (Supplementary Fig. 8*C*).

Ad-29cM/204I local vascular release almost abolished neointimal formation (neointima/media areas ratio [N/M]: T1DM rats 0.46 ± 0.07; T2DM rats 0.56 ± 0.09) 14 days after injury when compared with Ad-NC–treated diabetic rats (N/M: T1DM 1.81 ± 0.192; T2DM 1.73 ± 0.168) (Fig. 7*C* and *D*). Furthermore, Ad-29cM/204I in T1DM and T2DM significantly reduced neointimal formation even when compared with Ad-NC–treated euglycemic controls (N/M 1.21 ± 0.2) (Fig. 7*C* and *D*). On the contrary, contemporary miR-29c-inhibitor and miR-204-mimic cotransfection in injured vessels of euglycemic rats increased neointima formation when compared with control-transfected vessels (Supplementary Fig. 8*D*).

Finally, in order to further explore the role of the CAV1 modulation in the injured diabetic artery, we first transduced VSMCs with a recombinant Ad-si*Cav1* infection in vitro. Ad-si*Cav1* reduced CAV1 protein levels despite contemporary miR-29c upregulation/miR-204 inhibition when compared with VSMCs transfected with appropriate controls (Supplementary Fig. 8*E*). Ad-29cM/204I and Ad-si*Cav1* cotransduction fostered a significant increase of EdU incorporation in VSMCs compared with the cells infected with Ad-29cM/204I (Supplementary Fig. 9*A*). We eventually assessed the effect of Ad-si*Cav1* and Ad-29cM/204I coinfection on neointimal formation in injured arteries from T1DM and T2DM rats. As shown in Supplementary Fig. 9*B*, concomitant Ad-29cM/204I and Ad-si*Cav1* infection reduced CAV1 levels 48 h after balloon injury both in T1DM and T2DM carotid arteries when compared with the injured artery infected with Ad-29cM/204I. Importantly, *Cav1* inhibition by Ad-si*Cav1* increased neointima formation of both T1DM and T2DM carotid arteries transfected with Ad-29cM/204I when compared with injured arteries infected with Ad-29cM/204I + Ad-siNC (Supplementary Fig. 9*C*).

Therefore, miR-29c and miR-204 are central Diab-miRs forming with their targets, EMP2 and CAV1, a molecular network that has a critical role in regulating the exaggerated detrimental VSMC phenotypic switch in DM.

DISCUSSION

The main findings emanating from this study are as follows: *1*) the diabetic detrimental hyperplastic phenotype of VSMCs is characterized by an miRNA signature that diverges significantly from the miRNA network activated in ND VSMCs; *2*) this miRNA signature is integrated in an miRNA-mRNA network that regulates gene cascades involved in various aspects of VSMC phenotypic switch upon vascular injury; and *3*) miR-29c and miR-204 comodulation, and their molecular targets Emp2 and CAV1, are necessary in regulating diabetic VSMC proliferation in vitro and in vivo.

miRNAs are key controllers of several pathophysiological conditions and clinically specific biomarkers for various diseases (37). Patients with diabetes display a significant deregulation of miRNAs involved in angiogenesis, vascular repair, and endothelial homeostasis (38). VSMC phenotypic switch is a key cellular event in vasculoproliferative disorders (39,40), and VSMCs display a different and more aggressive phenotype in patients with diabetes (9–12). miRNAs play key roles in VSMC functions, but their role under diabetic conditions is unclear. Recently, small RNA-Seq identified several differentially expressed miRNAs in VSMCs from T2DM *db*/*db* mice versus ND *db*/+ mice (17). However, the study was not designed to specifically address VSMC phenotypic switch, and it did not assess miRNA expression upon vascular injury. Here, assessing the whole miRNome in diabetic injured versus uninjured vascular tissues, we identified a group of six miRNAs consistently showing robust deregulation in diabetic conditions. These Diab-miRs were similarly deregulated in human diabetic atherosclerotic plaques and coronary SMCs. miR-29c and miR-204 were studied in detail, because of their more pronounced dysregulation and robust effects on VSMC proliferation in vitro.

miR-29c is part of the miR-29 gene family, which has been extensively investigated in many types of cancers (41,42). Also, miR-29 is involved in the pathogenesis of kidney disease (43), where renoprotective drugs act through an increase of miR-29 expression (44). Importantly, individual members of the miR-29 gene family also function as regulators of vascular cells. In particular, miR-29b promotes VSMC differentiation from embryonic stem cells by targeting YY1 (Yin Yang 1), a transcription factor that inhibits muscle cell differentiation and muscle-specific gene expression (45). In addition, other examples of the roles of the miR-29 gene family in mediating phenotypic modulation of vascular cells have been reported (46,47). miR-204 plays a significant role in the development of eyes (48) and adipogenesis (49). It is believed that miR-204 acts mainly as a tumor suppressor; however, it has been shown that its function can also evolve to that of an oncomiR in certain instances (50). Of note, miR-204 overexpression plays a critical role in the development of diabetes (51).

Here we show that miR-29c upregulation and miR-204 downregulation inhibit VSMC proliferation in DM in vitro and in vivo. Their effect is additive because their simultaneous modulation to increase miR-29c and inhibit

204 abolishes the detrimental and exaggerated hyperplastic response of VSMCs in DM after vascular injury. miR-29c directly targets for repression *Emp2* while miR-204 targets *Cav1*. A single miRNA has multiple mRNA targets, and often these multiple targets converge to regulate the same molecular and cellular process (52), whereas multiple miRNAs can converge on the same pathway, fine-tuning its activity via one or more mRNAs (53). The latter appears to be functioning in the combined effects of miR-29c and miR-204. miR-29c targets for *Emp2* repression, which in turn regulates *Cav1*, which is a target of miR-204. In particular, miR-204 fine-tunes *Cav1* protein expression without degrading its mRNA. The combined gene repression and fine-tuning effects of these miRNAs are necessary to promote the detrimental VSMC diabetic phenotype. Thus, we discovered an miRNA-mRNA-protein molecular network that is an essential to prevent vasculoproliferative response in DM in vivo.

Treatment of atherosclerotic lesions in coronary and peripheral artery diseases is still a challenge in patients with DM. It highly tempting to speculate that miR-29c and miR-204 comodulation may represent a more tailored and specific therapy for a local release approach to prevent vascular sequels in the treatment of vasculoproliferative diseases in diabetes.

Funding. This work was supported by grants PRIN2015 2015ZTT5KB_004 and FIRB-Futuro-in-Ricerca (RBFR12I3KA) Flagship Project InterOmics from the Italian Ministry of Education, University and Research; Finalized Research2010 (GR-2010-2318945) from the Italian Ministry of Health; and Investigator Grant (IG-17426) from Italian Association for Cancer Research.

Duality of Interest. No potential conflicts of interest relevant to this article were reported.

Author Contributions. D.T. designed the research, supervised the experiments, and wrote the manuscript. C.Ia., F.M., C.Ve., I.A., M.S., T.M., E.C., C.Va., P.M., L.T., and C.Vi. conducted the experiments and analyzed the data. R.T., G.G., and A.W. conducted the RNA-Seq experiments. F.C.S., D.C., and M.T. contributed reagents. C.In. contributed to discussion and reviewed the manuscript. D.T. and C.In. are the guarantors of this work and, as such, had full access to all the data in the study and take responsibility for the integrity of the data and the accuracy of the data analysis.

References

1. Ding Y, Zhang M, Zhang W, et al. AMP-activated protein kinase alpha 2 deletion induces VSMC phenotypic switching and reduces features of atherosclerotic plaque stability. Circ Res 2016;119:718–730

2. Alexander MR, Owens GK. Epigenetic control of smooth muscle cell differentiation and phenotypic switching in vascular development and disease. Annu Rev Physiol 2012;74:13–40

3. Shankman LS, Gomez D, Cherepanova OA, et al. KLF4-dependent phenotypic modulation of smooth muscle cells has a key role in atherosclerotic plaque pathogenesis. Nat Med 2015;21:628–637

4. Horita H, Wysoczynski CL, Walker LA, et al. Nuclear PTEN functions as an essential regulator of SRF-dependent transcription to control smooth muscle differentiation. Nat Commun 2016;7:10830

5. Torella D, Curcio A, Gasparri C, et al. Fludarabine prevents smooth muscle proliferation in vitro and neointimal hyperplasia in vivo through specific inhibition of STAT-1 activation. Am J Physiol Heart Circ Physiol 2007;292:H2935–H2943

6. Bennett MR, Sinha S, Owens GK. Vascular smooth muscle cells in atherosclerosis. Circ Res 2016;118:692–702

7. Porter KE, Riches K. The vascular smooth muscle cell: a therapeutic target in type 2 diabetes? Clin Sci (Lond) 2013;125:167–182

8. Madi HA, Riches K, Warburton P, O'Regan DJ, Turner NA, Porter KE. Inherent differences in morphology, proliferation, and migration in saphenous vein smooth muscle cells cultured from nondiabetic and type 2 diabetic patients. Am J Physiol Cell Physiol 2009;297:C1307–C1317

9. Faries PL, Rohan DI, Takahara H, et al. Human vascular smooth muscle cells of diabetic origin exhibit increased proliferation, adhesion, and migration. J Vasc Surg 2001;33:601–607

10. Zhang X, Liu L, Chen C, et al. Interferon regulatory factor-1 together with reactive oxygen species promotes the acceleration of cell cycle progression by up-regulating the cyclin E and CDK2 genes during high glucose-induced proliferation of vascular smooth muscle cells. Cardiovasc Diabetol 2013;12:147

11. Wang CC, Gurevich I, Draznin B. Insulin affects vascular smooth muscle cell phenotype and migration via distinct signaling pathways. Diabetes 2003;52:2562–2569

12. Engberding N, San Martín A, Martin-Garrido A, et al. Insulin-like growth factor-1 receptor expression masks the antiinflammatory and glucose uptake capacity of insulin in vascular smooth muscle cells. Arterioscler Thromb Vasc Biol 2009;29:408–415

13. Torella D, Iaconetti C, Catalucci D, et al. MicroRNA-133 controls vascular smooth muscle cell phenotypic switch in vitro and vascular remodeling in vivo. Circ Res 2011;109:880–893

14. Nassa G, Tarallo R, Giurato G, et al. Post-transcriptional regulation of human breast cancer cell proteome by unliganded estrogen receptor β via microRNAs. Mol Cell Proteomics 2014;13:1076–1090

15. Iaconetti C, De Rosa S, Polimeni A, et al. Down-regulation of miR-23b induces phenotypic switching of vascular smooth muscle cells in vitro and in vivo. Cardiovasc Res 2015;107:522–533

16. Santulli G, Wronska A, Uryu K, et al. A selective microRNA-based strategy inhibits restenosis while preserving endothelial function. J Clin Invest 2014;124:4102–4114

17. Reddy MA, Das S, Zhuo C, et al. Regulation of vascular smooth muscle cell dysfunction under diabetic conditions by miR-504. Arterioscler Thromb Vasc Biol 2016;36:864–873

18. Indolfi C, Torella D, Cavuto L, et al. Effects of balloon injury on neointimal hyperplasia in streptozotocin-induced diabetes and in hyperinsulinemic non-diabetic pancreatic islet-transplanted rats. Circulation 2001;103:2980–2986

19. Dago DN, Scafoglio C, Rinaldi A, et al. Estrogen receptor beta impacts hormone-induced alternative mRNA splicing in breast cancer cells. BMC Genomics 2015;16:367

20. Cimmino G, Tarallo R, Nassa G, et al. Activating stimuli induce platelet microRNA modulation and proteome reorganisation. Thromb Haemost 2015;114:96–108

21. Ravo M, Cordella A, Rinaldi A, et al. Small non-coding RNA deregulation in endometrial carcinogenesis. Oncotarget 2015;6:4677–4691

22. Panero R, Rinaldi A, Memoli D, et al. iSmaRT: a toolkit for a comprehensive analysis of small RNA-Seq data. Bioinformatics 2017;33:938–940

23. Tarallo R, Giurato G, Bruno G, et al. The nuclear receptor ERβ engages AGO2 in regulation of gene transcription, RNA splicing and RISC loading. Genome Biol 2017;18:189

24. Curcio A, Torella D, Iaconetti C, et al. MicroRNA-1 downregulation increases connexin 43 displacement and induces ventricular tachyarrhythmias in rodent hypertrophic hearts. PLoS One 2013;8:e70158

25. Jonas M, Edelman ER, Groothuis A, Baker AB, Seifert P, Rogers C. Vascular neointimal formation and signaling pathway activation in response to stent injury in insulin-resistant and diabetic animals. Circ Res 2005;97:725–733

26. Liu X, Cheng Y, Zhang S, Lin Y, Yang J, Zhang C. A necessary role of miR-221 and miR-222 in vascular smooth muscle cell proliferation and neointimal hyperplasia. Circ Res 2009;104:476–487

27. Ji R, Cheng Y, Yue J, et al. MicroRNA expression signature and antisense-mediated depletion reveal an essential role of MicroRNA in vascular neointimal lesion formation. Circ Res 2007;100:1579–1588
28. Wamhoff BR, Hoofnagle MH, Burns A, Sinha S, McDonald OG, Owens GK. A G/C element mediates repression of the SM22alpha promoter within phenotypically modulated smooth muscle cells in experimental atherosclerosis. Circ Res 2004;95:981–988
29. Little PJ, Allen TJ, Hashimura K, Nigro J, Farrelly CA, Dilley RJ. High glucose potentiates mitogenic responses of cultured ovine coronary smooth muscle cells to platelet derived growth factor and transforming growth factor-beta1. Diabetes Res Clin Pract 2003;59:93–101
30. Morales SA, Mareninov S, Coulam P, et al. Functional consequences of interactions between FAK and epithelial membrane protein 2 (EMP2). Invest Ophthalmol Vis Sci 2009;50:4949–4956
31. Fu M, Rao R, Sudhakar D, et al. Epithelial membrane protein-2 promotes endometrial tumor formation through activation of FAK and Src. PLoS One 2011;6:e19945
32. Liu HM, Zhao XF, Guo LN, Tan Z, Wang TH. Effects of caveolin-1 on the 17beta-estradiol-mediated inhibition of VSMC proliferation induced by vascular injury. Life Sci 2007;80:800–812
33. Carrillo-Sepulveda MA, Matsumoto T. Phenotypic modulation of mesenteric vascular smooth muscle cells from type 2 diabetic rats is associated with decreased caveolin-1 expression. Cell Physiol Biochem 2014;34:1497–1506
34. Wan X, Chen Z, Choi WI, Gee HY, Hildebrandt F, Zhou W. Loss of epithelial membrane protein 2 aggravates podocyte injury via upregulation of caveolin-1. J Am Soc Nephrol 2016;27:1066–1075
35. Forbes A, Wadehra M, Mareninov S, et al. The tetraspan protein EMP2 regulates expression of caveolin-1. J Biol Chem 2007;282:26542–26551
36. Hall DP, Cost NG, Hegde S, et al. TRPM3 and miR-204 establish a regulatory circuit that controls oncogenic autophagy in clear cell renal cell carcinoma. Cancer Cell 2014;26:738–753
37. Thum T, Condorelli G. Long noncoding RNAs and microRNAs in cardiovascular pathophysiology. Circ Res 2015;116:751–762
38. Paneni F, Beckman JA, Creager MA, Cosentino F. Diabetes and vascular disease: pathophysiology, clinical consequences, and medical therapy: part I. Eur Heart J 2013;34:2436–2443
39. Torella D, Gasparri C, Ellison GM, et al. Differential regulation of vascular smooth muscle and endothelial cell proliferation in vitro and in vivo by cAMP/PKA-activated p85alphaPI3K. Am J Physiol Heart Circ Physiol 2009;297:H2015–H2025
40. Nguyen AT, Gomez D, Bell RD, et al. Smooth muscle cell plasticity: fact or fiction? Circ Res 2013;112:17–22
41. Wang B, Li W, Liu H, et al. miR-29b suppresses tumor growth and metastasis in colorectal cancer via downregulating Tiam1 expression and inhibiting epithelial-mesenchymal transition. Cell Death Dis 2014;5:e1335
42. Amodio N, Rossi M, Raimondi L, et al. miR-29s: a family of epi-miRNAs with therapeutic implications in hematologic malignancies. Oncotarget 2015;6:12837–12861
43. Fang Y, Yu X, Liu Y, et al. miR-29c is downregulated in renal interstitial fibrosis in humans and rats and restored by HIF-α activation. Am J Physiol Renal Physiol 2013;304:F1274–F1282
44. Chen H-Y, Zhong X, Huang XR, et al. MicroRNA-29b inhibits diabetic nephropathy in db/db mice. Mol Ther 2014;22:842–853
45. Jin M, Wu Y, Wang Y, et al. MicroRNA-29a promotes smooth muscle cell differentiation from stem cells by targeting YY1. Stem Cell Res (Amst) 2016;17:277–284
46. Boon RA, Seeger T, Heydt S, et al. MicroRNA-29 in aortic dilation: implications for aneurysm formation. Circ Res 2011;109:1115–1119
47. Bretschneider M, Busch B, Mueller D, et al. Activated mineralocorticoid receptor regulates micro-RNA-29b in vascular smooth muscle cells. FASEB J 2016;30:1610–1622
48. Conte I, Carrella S, Avellino R, et al. miR-204 is required for lens and retinal development via Meis2 targeting. Proc Natl Acad Sci U S A 2010;107:15491–15496
49. Huang J, Zhao L, Xing L, Chen D. MicroRNA-204 regulates Runx2 protein expression and mesenchymal progenitor cell differentiation. Stem Cells 2010;28:357–364
50. Li T, Pan H, Li R. The dual regulatory role of miR-204 in cancer. Tumour Biol 2016;37:11667–11677
51. Xu G, Chen J, Jing G, Shalev A. Thioredoxin-interacting protein regulates insulin transcription through microRNA-204. Nat Med 2013;19:1141–1146
52. Selbach M, Schwanhäusser B, Thierfelder N, Fang Z, Khanin R, Rajewsky N. Widespread changes in protein synthesis induced by microRNAs. Nature 2008;455:58–63
53. Schmiedel JM, Klemm SL, Zheng Y, et al. Gene expression. MicroRNA control of protein expression noise. Science 2015;348:128–132